Site-Specific Effects of Zinc on the Activity of Family II Pyrophosphatase†

Anton B. Zyryanov,‡ Marko Tammenkoski,§ Anu Salminen,§ Galina Ya. Kolomiytseva,‡ Igor P. Fabrichniy,# Adrian Goldman,# Reijo Lahti,*,§ and Alexander A. Baykov*,‡

A. N. Belozersky Institute of Physico-Chemical Biology and School of Chemistry, Moscow State University, Moscow 119899, Russia, Department of Biochemistry, University of Turku, FIN-20014 Turku, Finland, and Institute of Biotechnology, University of Helsinki, P.O. Box 56, FIN-00014 Helsinki, Finland

Received July 18, 2004; Revised Manuscript Received September 10, 2004

ABSTRACT: Family II pyrophosphatases (PPases), recently found in bacteria and archaebacteria, are Mn^{2+}-containing metalloenzymes with two metal-binding subsites (M1 and M2) in the active site. These PPases can use a number of other divalent metal ions as the cofactor but are inactive with Zn^{2+}, which is known to be a good cofactor for family I PPases. We report here that the Mg^{2+}-bound form of the family II PPase from *Streptococcus gordonii* is nearly instantly activated by incubation with equimolar Zn^{2+}, but the activity thereafter decays on a time scale of minutes. The activation of the Mn^{2+}-form by Zn^{2+} was slower but persisted for hours, whereas activation was not observed with the Ca^{2+}- and apo-forms. The bound Zn^{2+} could be removed from PPase by prolonged EDTA treatment, with a complete recovery of activity. On the basis of the effect of Zn^{2+} on PPase dimerization, the Zn^{2+} binding constant appeared to be as low as 10^{-12} M for *S. gordonii* PPase. Similar effects of Zn^{2+} and EDTA were observed with the Mg^{2+}- and apo-forms of *Streptococcus mutans* and *Bacillus subtilis* PPases. The effects of Zn^{2+} on the apo- and Mg^{2+}-forms of HQ97 and DE15 *B. subtilis* PPase variants (modified M2 subsite) but not of HQ9 variant (modified M1 subsite) were similar to that for the Mn^{2+}-form of wild-type PPase. These findings can be explained by assuming that (a) the PPase tightly binds Mg^{2+} and Mn^{2+} at the M2 subsite; (b) the activation of the corresponding holoenzymes by Zn^{2+} results from its binding to the M1 subsite; and (c) the subsequent inactivation of Mg^{2+}-PPase results from Zn^{2+} migration to the M2 subsite. The inability of Zn^{2+} to activate apo-PPase suggests that Zn^{2+} binds more tightly to M2 than to M1, allowing direct binding to M2. Zn^{2+} is thus an efficient cofactor at subsite M1 but not at subsite M2.

A number of ATP-consuming reactions, such as protein, nucleic acid, and phospholipid syntheses, yield PP_i[1] as a byproduct. Soluble PPases convert this PP_i into P_i, thereby driving these biosynthetic reactions to completion (*1*). In addition, membrane-bound PPases couple PP_i hydrolysis to proton transport (*2*). PP_i hydrolysis is thus an essential biochemical reaction, which explains why PPases are found in all types of cells and in all species.

Soluble PPases comprise two families, denoted I and II, with completely different primary structures. Family I PPases, which have been known for about 70 years and are found in all types of organisms, are among the best characterized phosphoryl transfer enzymes (*3*, *4*). Family I PPases are homodimers (in eukaryotes) or homohexamers (in prokaryotes) of compact, one-domain subunits. Family II PPases were only recently found in bacteria and archaebacteria (*5*, *6*), often pathogenic, and have been only partially characterized. All known family II PPases are homodimers of two-domain subunits, interacting through N-terminal domains (*7*, *8*). The N- and C-terminal domains are linked by a flexible linker, allowing them to move by tens of angstroms relative to each other. The active site, located between the domains, undergoes profound structural changes as a result of this movement.

The properties of the two families also differ substantially. Family II PPases are 20- to 50-fold more active and exhibit different substrate and metal cofactor specificities. Unlike family I PPases, they do not hydrolyze ATP or other organic polyphosphates (*9*), prefer Mn^{2+} to Mg^{2+} as the cofactor (*4*, *5*), and are not inhibited by Ca^{2+} (*10*).

Divalent metal ion cofactors bind to multiple binding subsites and play dual roles in family II PPases. First, metal ions markedly stabilize the otherwise unstable dimeric structure of family II PPases by binding to one high-affinity subsite per subunit (*10*, *11*). The affinity of this subsite for Mn^{2+} and Co^{2+} is characteristic of metalloenzymes (K_d = 0.2 to 0.7 nM) (*10*, *11*), and these metals can be only removed by incubation with EDTA (*3*, *10*−*12*). This high-affinity subsite also binds Mg^{2+} and Ca^{2+}, although with a much lower affinity (*10*, *11*). Second, the metal ions bound to this and two lower affinity subsites are directly involved

† This work was supported by grants from the Russian Foundation for Basic Research (03-04-48798), the Ministry of Industry, Science and Technologies of the Russian Federation (1706-2003-4), the Finnish Academy of Sciences (201611, 172618, and 168155), and Sigrid Juselius Foundation, Biocentrum Helsinki.

* To whom correspondence should be addressed. A.A.B. (Tel 095-939-5541; fax 095-939-3181; e-mail baykov@genebee.msu.su) and R.L. (Tel 358-2-333-6845; fax 358-2-333-6860; e-mail reijo.lahti@utu.fi).

‡ Moscow State University.

§ University of Turku.

University of Helsinki.

[1] Abbreviations: *bs*PPase, *Bacillus subtilis* inorganic pyrophosphatase; PPase, inorganic pyrophosphatase; P_i, inorganic phosphate; PP_i, inorganic pyrophosphate; *sg*PPase, *Streptococcus gordonii* inorganic pyrophosphatase; *sm*PPase, *Streptococcus mutans* inorganic pyrophosphatase.

10.1021/bi048470j CCC: $27.50
Published on Web 10/23/2004

in catalysis by interacting with the substrate and, probably, the nucleophilic water (*7*, *8*). In *Streptococcus gordonii*, the effectiveness of different divalent metal ions in this respect is $Mn^{2+} > Co^{2+} > Mg^{2+} > Ca^{2+}$ (*11*). The family II PPase from *Methanococcus jannaschii* exhibits a somewhat different metal cofactor specificity and appears to be activated most effectively by Co^{2+} in combination with Mg^{2+} (*13*). Finally, Zn^{2+} has been reported to be ineffective as a cofactor for *Bacillus subtilis* PPase (*bs*PPase) (*12*) and to inhibit Co^{2+}-activated *M. jannaschii* PPase (*13*).

The very large difference in the binding affinities between the high-affinity subsite and the lower affinity subsites allows one to vary the metal ion at the high-affinity subsite while keeping the other subsites filled with Mg^{2+}. Such mixed cofactor assays have indicated that the high-affinity subsite is the main determinant of the catalytic properties of the PPase. Thus, *Streptococcus gordonii* PPase (*sg*PPase) is inactive with Ca^{2+} bound to all the subsites, but exhibits substantial activity with Mn^{2+} at the high-affinity subsite and Ca^{2+} at the other subsites (*10*). Interestingly, fluoride is a potent inhibitor of the all-Mg^{2+}-form of this enzyme but is ineffective when the high-affinity subsite is occupied with Mn^{2+} or Co^{2+} (*10*, *13*). Consequently, the fluoride in toothpaste cannot inhibit the PPase of *Streptococcus mutans* (*sm*PPase), the bacterium that causes dental caries, because it accumulates protecting Mn^{2+} (*14*, *15*).

In our most recent study (*11*), we were able to determine the rate constants for all individual reaction steps catalyzed by *sg*PPase with Mn^{2+}, Co^{2+}, or Mg^{2+} at the high-affinity subsite and Mg^{2+} at all other subsites. These results demonstrated that the marked acceleration of *sg*PPase catalysis upon Mn^{2+} and Co^{2+} binding at the high-affinity subsite results from a combined effect of these ions on the hydrolysis and the release of bound P_i.

The present study examines the ability of Zn^{2+} to act as a cofactor of family II PPases. We show that Zn^{2+} can partially act as a cofactor, but only in combination with Mn^{2+}. The activation by Zn^{2+} in the presence of Mg^{2+} is only transient and is followed by a decay of activity to nearly zero. Using site-directed mutagenesis in combination with functional studies, we elucidate the mechanism behind this unusual behavior.

EXPERIMENTAL PROCEDURES

Enzyme. The bacterial PPases, *bs*PPase, *sg*PPase, and *sm*PPase were expressed in *Escherichia coli* C43(DE3) and purified as described previously (*10*). Site-directed mutagenesis was performed with a QuikChange mutagenesis kit (Stratagene, La Jolla, CA).

Metal-free PPase (apo-PPase) was prepared by EDTA treatment of the PPase followed by ultrafiltration on a Centricon SR30 membrane (30-kDa cutoff). Before use, the membrane was soaked in 25 mM sodium EDTA, pH 7.2, washed with 10 mM EDTA (pH 7.2) and, finally, with 10 μM EDTA. Stock enzyme solution containing 2 to 5 mM enzyme, 150 mM Tris-Cl (pH 7.2), 1.5 mM $MnCl_2$, and 15 mM $MgCl_2$ was diluted to 100 μM enzyme with 72 mM Hepes-KOH (pH 7.2) containing 28 mM KCl and 2 mM EDTA. The resulting solution was subjected to three cycles of 20- to 40-fold dilution followed by ultrafiltration with the Centricon membrane. The EDTA concentration in the dilution buffer was 2 mM for the first two cycles and 20 to 50 mM for the third cycle. After the third cycle, the diluted enzyme solution was incubated with 20 to 50 mM EDTA for 3 days at 25 °C and then subjected to six further cycles of concentration and dilution in 10 μM EDTA. The final solution was adjusted to 1 to 2 mM enzyme and stored at 4 °C. Except where indicated, the Zn^{2+}-form of *sg*PPase (Zn-*sg*PPase) was prepared by incubating 26 μM metal-free enzyme with 30 μM $ZnCl_2$ for at least 10 h at 25 °C in 72 mM Hepes-KOH (pH 7.2) containing 28 mM KCl.

The enzyme concentration was calculated as the subunit concentration on the basis of a subunit molecular mass of 33.5 kDa (*10*) and an extinction coefficient $A_{280}^{1\%}$ of 2.62 (*11*).

Analytical Procedures. Except as noted, all measurements were performed at 25 °C in 72 mM Hepes-KOH buffer (pH 7.2) containing 28 mM KCl.

PP_i-hydrolyzing activity was assayed using an automatic phosphate analyzer (*16*). PP_i hydrolysis was initiated by addition of the enzyme to 5 to 25 mL of 150 mM Tris-Cl buffer (pH 7.2) containing 50 to 57 μM PP_i and 0.17 mM $MnCl_2$, 22 mM $CaCl_2$, or 20 mM $MgCl_2$. To determine Michaelis−Menten parameters, PP_i concentration was varied in the range of 10−500 μM. The reaction was monitored for 3 to 4 min. Assays using Ca^{2+} or Mg^{2+} as the metal cofactors also included 2 mM EDTA or 0.5 mM EGTA, respectively.

Sedimentation velocity measurements were performed on a Spinco E analytical ultracentrifuge (Beckman Instruments, Palo Alto, CA) at 48 000 rpm with scanning at 280 nm. The sedimentation coefficient, $s_{20,w}$, was calculated according to standard procedures (*17*). Prior to the sedimentation analysis, the enzyme was incubated in the appropriate medium for at least 1 day.

Zn^{2+} concentrations were determined by atomic absorption spectroscopy at 213 nm using a Kvant-AFA instrument (ZAO Aquilon, Moscow).

Calculations and Data Analysis. (a) Time Course of Zinc Removal from PPase. EDTA-induced Zn^{2+} removal from PPase can be described by Scheme 1, which assumes that Zn^{2+} removal from each enzyme subunit occurs independently as a first-order reaction with a rate constant k_r.

On the basis of this scheme, the concentrations of different enzyme species as a function of time are given by eqs 1−3, where $[E]_t$ is total enzyme concentration.

$$\frac{d[E_2Zn_2]}{dt} = -2k_r[E_2Zn_2] \quad (1)$$

$$\frac{d[E_2Zn]}{dt} = -k_r[E_2Zn] + 2k_r[E_2Zn_2] \quad (2)$$

$$[E]_t = 2([E_2Zn_2] + [E_2Zn] + [E_2]) \quad (3)$$

The specific activity of PPase upon addition of the mixture of enzyme species (see Scheme 1) to the Mn^{2+}-containing activity assay medium is described by

$$A = \frac{A_{mn}([E] + 2[E_2]) + A_{zn}([E_2Zn] + 2[E_2Zn_2]) + A_{mn/zn}[E_2Zn]}{[E]_t} \quad (4)$$

Scheme 1

$$E_2Zn_2 \xrightarrow{2k_r} E_2Zn \xrightarrow{k_r} E_2$$

Scheme 2: Zinc Binding to the High-Affinity Subsite of PPase[a]

$$2E + 2Zn \overset{K_d}{\leftrightarrows} E_2 + 2Zn \overset{1/2K_M}{\leftrightarrows} E_2Zn + Zn \overset{2K_M}{\leftrightarrows} E_2Zn_2$$

[a] E and E_2 are enzyme monomer and dimer, respectively; K_d and K_M are dissociation constants for the corresponding equilibria.

where A is the measured specific activity of the PPase; A_{mn} and $A_{mn/zn}$ are specific activities of the Zn^{2+}-free subunit of the dimer without or with Zn^{2+} bound to the other subunit, respectively; A_{zn} is the specific activity of the Zn^{2+}-bound subunit; and $[E]_t$ is the total concentration of enzyme subunits. Equation 4 implies that the activity of the Zn^{2+}-free subunit depends on whether Zn^{2+} is present in the other subunit.

(b) Estimation of Equilibrium Zn^{2+} Binding to sgPPase Based on the Stimulation of Dimerization. The equilibria in the system containing *sg*PPase and Zn^{2+} are shown in Scheme 2, which is based on previous measurements of the binding of other metal ions to family II PPases (*10*, *11*). It implies that Zn^{2+} binds only to dimeric *sg*PPase, thereby stimulating dimerization. In this scheme, K_M is a microscopic dissociation constant, and $1/2K_M$ and $2K_M$ are the corresponding macroscopic constants for metal binding to two identical sites in the dimer (*18*). EGTA was added to buffer the free Zn^{2+} concentration, and its complex with Zn^{2+} at pH 7.2 was taken into account by using a dissociation constant, K_{egta}, of 1 nM, which was derived from the respective pH-independent constant (*19*).

The concentrations of free metal ion, [Zn], and all enzyme species shown in Scheme 2 were obtained by solving eqs 5−9, where $[Zn]_t$ and $[EGTA]_t$ are the total Zn^{2+} and EGTA concentrations, respectively. The K_d value was fixed at 120 μM, as determined previously (*11*).

$$[E] = \frac{K_M\left(\sqrt{K_d(8[E]_t([Zn] + K_M)^2 + K_dK_M{}^2)} - K_dK_M\right)}{4(K_M + [Zn])^2} \quad (5)$$

$$[E_2] = \frac{[E]^2}{K_d} \quad (6)$$

$$[E_2Zn] = 2\frac{[Zn][E]^2}{K_MK_d} \quad (7)$$

$$[E_2Zn_2] = \frac{[Zn]^2[E]^2}{K_M{}^2K_d} \quad (8)$$

$$[Zn]_t = [Zn] + 2\frac{[Zn][E]^2}{K_MK_d} + 2\frac{[Zn]^2[E]^2}{K_M{}^2K_d} + \frac{[Zn][EGTA]_t}{K_{egta} + [Zn]} \quad (9)$$

Equation 4 gives the specific activity of *sg*PPase upon addition of the equilibrium mixture containing the enzyme species shown in Scheme 2 to the activity assay medium. The use of eq 4 in this case implies that the monomeric enzyme is converted into the dimer upon binding the metal cofactor (Mn^{2+}) in the assay medium (*10*) and that the activity of the Zn^{2+}-free subunit depends on whether Zn^{2+} is present in the other subunit. Nonlinear least-squares fitting of the data was performed using SCIENTIST version 2.01 (Micromath), which allows the use of implicit equations.

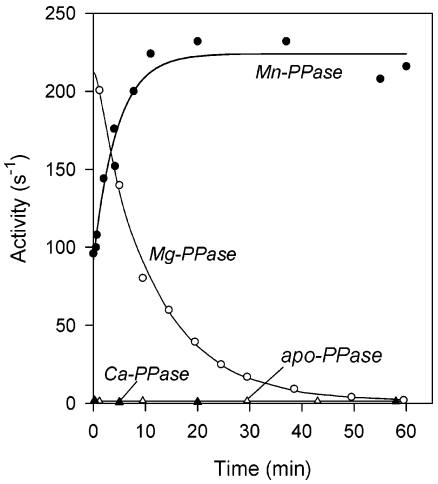

FIGURE 1: Time course of PPase activity upon addition of 26 μM apo-*sg*PPase, Ca-*sg*PPase, Mg-*sg*PPase, or Mn-*sg*PPase to a solution of 30 μM $ZnCl_2$. Aliquots were withdrawn at the indicated times, and PPase activity was assayed with Ca^{2+} as the cofactor. Mg-*sg*PPase was obtained by incubation of 2 mM apo-*sg*PPase with 2.1 mM $MgCl_2$ for 3 days. Ca-*sg*PPase and Mn-*sg*PPase were obtained by a 2-h incubation of 0.75 mM apo-*sg*PPase with 2 mM $CaCl_2$ and 2 mM $MnCl_2$, respectively. Assuming 1:1 binding, the unbound concentrations of Mg^{2+}, Ca^{2+}, and Mn^{2+} during the incubation with Zn^{2+} were 1.3, 44, and 44 μM, respectively. The lines for Mg-*sg*PPase and Mn-*sg*PPase were obtained using eq 10 and the best-fit parameter values given in Table 1.

RESULTS

Transient Activation of Mg-sgPPase by Zn^{2+}. Interaction of *sg*PPase with an equimolar concentration of Zn^{2+} can produce different Zn^{2+}-bound forms of this enzyme. The zinc form (Zn-*sg*PPase) that arises within 10 s of addition of Zn^{2+} to the apoenzyme (apo-*sg*PPase) is characterized by low (1.4 s^{-1}) and constant activity (Figure 1). A second form (Zn-*sg*PPase*) that is much more active (200 s^{-1}) is transiently formed upon addition of Zn^{2+} to *sg*PPase that has been preincubated with Mg^{2+} (Mg-*sg*PPase). This second form is initially a dimer because it has Mg^{2+} in the M1 subsite. The final activity values were identical for the apo- and Mg-*sg*PPase, indicating that the more active Zn-*sg*PPase* is converted into the less active Zn-*sg*PPase. Importantly, dilution of Mg-*sg*PPase into metal-free buffer has been shown to immediately result in zero activity (<0.1 s^{-1}) when measured with Ca^{2+} as the cofactor because Mg-*sg*PPase is inactive with Ca^{2+} (*10*). Therefore, the activity burst seen in Figure 1 clearly results from Zn^{2+} binding to *sg*PPase.

The conversion of Zn-*sg*PPase* into Zn-*sg*PPase could be described by the following equation for a first-order reaction:

$$A = A_{zn} + (A_{zn*} - A_{zn})e^{-k_ct} \quad (10)$$

where A is the measured activity; A_{zn*} and A_{zn} are the activities of Zn-*sg*PPase* and Zn-*sg*PPase, respectively; and k_c is the rate constant for the interconversion. The values of A_{zn*} and A_{zn} were proportional to the concentration of Zn^{2+}

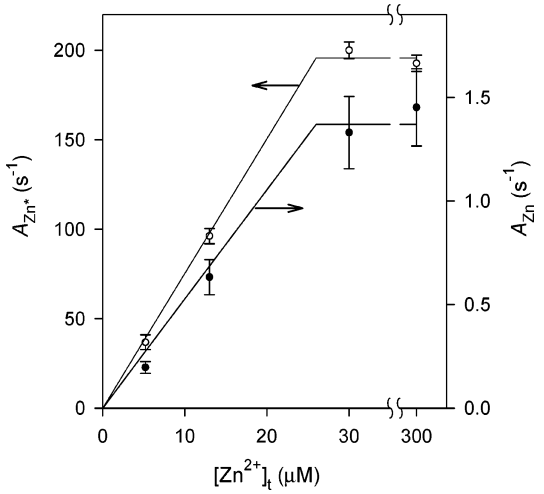

FIGURE 2: The dependence of A_{zn*} and A_{zn} for Mg-*sg*PPase on the concentration of added $ZnCl_2$. The experiment was performed as described in Figure 1.

Table 1: Parameters of Eq 10 as a Function of Assay Conditions[a]

starting enzyme	assay cofactor	A_{zn*} (s^{-1})	A_{zn} (s^{-1})	k_c (min^{-1})
Mg-*sg*PPase	Ca^{2+}	200 ± 20	1.4 ± 0.4	0.094 ± 0.005
Mg-*sg*PPase[b]	Ca^{2+}	230 ± 10	3 ± 2	0.068 ± 0.005
Mg-*sg*PPase	Mg^{2+}	180 ± 10	20 ± 2	0.101 ± 0.008
Mg-*sg*PPase	Mn^{2+}	460 ± 20	9 ± 2	0.089 ± 0.003
Mn-*sg*PPase	Ca^{2+}	92 ± 7	220 ± 10	0.22 ± 0.04
Mn-*sg*PPase[c]	Ca^{2+}	110 ± 20	200 ± 10	0.24 ± 0.10
Mn-*sg*PPase	Mn^{2+}	940 ± 50	1360 ± 40	nd[d]
Mg-*sm*PPase	Mn^{2+}	91 ± 2	12 ± 1	0.075 ± 0.003
Mg-*bs*PPase	Ca^{2+}	23 ± 1	3.7 ± 0.2	0.55 ± 0.04
Mg-*bs*PPase	Mn^{2+}	18 ± 1	8.0 ± 0.4	0.26 ± 0.04
Mn-*bs*PPase	Ca^{2+}	100 ± 20	310 ± 10	0.7 ± 0.2
HQ97-Mg-*bs*PPase	Mn^{2+}	2.3 ± 0.4	5.6 ± 0.4	0.17 ± 0.05
HQ98-Mg-*bs*PPase	Mn^{2+}	0.12 ± 0.01	0.03 ± 0.01	0.09 ± 0.03

[a] Assay cofactor concentration was 20 mM (Ca and Mg) or 0.17 mM (Mn). All assays contained 50−57 μM PP_i. [b] The enzyme was incubated with Zn^{2+} in the presence of 5 mM Mg^{2+}. [c] The enzyme was incubated with Zn^{2+} in the presence of 2 mM Ca^{2+}. [d] Not determined.

in the preincubation medium up to a [Zn]/[enzyme] ratio of about one, and, above this value, they remained constant (Figure 2). Thus, both Zn-*sg*PPase* and Zn-*sg*PPase must contain one Zn^{2+} ion per subunit.

The value of k_c was independent of the metal cofactor used in the activity assay, whereas the absolute values of A_{zn*} and A_{zn} varied depending on the metal cofactor used (Table 1). More importantly, changing the metal cofactor also affected the A_{zn}/A_{zn*} ratio, ruling out the possibility that Zn-*sg*PPase is inactive and that A_{zn} is entirely due to the presence of some Zn-*sg*PPase* in equilibrium with Zn-*sg*PPase. In the latter case, A_{zn}/A_{zn*} would not depend on the nature of the metal cofactor in the activity assay and would be determined exclusively by the position of the equilibrium between Zn-*sg*PPase and Zn-*sg*PPase* in the preincubation mixture. Obviously, the ratio [Zn-*sg*PPase]/[Zn-*sg*PPase*] at equilibrium cannot exceed 0.007, the lowest value of A_{zn}/A_{zn*}, observed with Ca^{2+} (the upper line in Table 1). Hence, the activity measured with Mg^{2+} as the cofactor (20 s^{-1}) is more than 93% due to Zn-*sg*PPase*. When 5 mM Mg^{2+} was added to the medium in which Mg-*sg*PPase was incubated with Zn^{2+}, there was a slight decrease in k_c (from 0.094 to 0.068 s^{-1}) but no significant change in A_{zn*} and A_{zn} (Table 1).

Table 2: Michaelis-Menten Parameters for Different Metal Forms of *sg*PPase[a]

	metal ion			
starting enzyme form	preincubation[b]	activity assay	K_m (μM)[c]	k_{cat} (s^{-1})
Mg-*sg*PPase	none	Mg^{2+}	9 ± 2	300 ± 20
Mg-*sg*PPase	Zn^{2+}	Mg^{2+}	87 ± 3	175 ± 10
Mn-*sg*PPase	none	Mg^{2+}	73 ± 8	2600 ± 100
Mn-*sg*PPase	Zn^{2+}	Mg^{2+}	26 ± 3	980 ± 30
Mn-*sg*PPase	none	Ca^{2+}	29 ± 4	146 ± 7
Mn-*sg*PPase	Zn^{2+}	Ca^{2+}	27 ± 5	360 ± 20

[a] Activity assays contained 20 mM $MgCl_2$ or $CaCl_2$, as indicated, and 0.15 M Tris-HCl, pH 7.2. [b] Preincubations with Zn^{2+} were performed as for Figure 1 for at least 1 h. [c] K_m values are in terms of total PP_i concentration.

A decay in activity was not observed when Mg-*sg*PPase was diluted into buffer containing Mn^{2+} or Co^{2+} instead of Zn^{2+}. With these metal ions, the final constant level of activity (1100 and 82 s^{-1}, respectively, when measured with Mg^{2+} as the cofactor) was attained within 30 s.

Effects of Zn^{2+} on Ca- and Mn-sgPPases. When *sg*PPase was preincubated with Ca^{2+} (Ca-*sg*PPase) instead of Mg^{2+}, it did not show an activity burst upon addition of Zn^{2+}, which is similar to the behavior of the apo-form (Figure 1). In contrast, *sg*PPase preincubated with Mn^{2+} (Mn-*sg*PPase) was activated 2.4-fold by Zn^{2+} with a rate constant of 0.22 min^{-1}. Unlike Mg-*sg*PPase, the activity remained constant for at least 2 h thereafter. The effect of Zn^{2+} binding to Mn-*sg*PPase was less pronounced if the activity was measured with Mn^{2+} as the cofactor (Table 1). Addition of 2 mM Ca^{2+} to the medium in which Mn-*sg*PPase was incubated with Zn^{2+} had only a small effect on k_c, A_{zn}, and A_{zn*} (Table 1).

Catalytic and Structural Characteristics of Zn-sgPPase. After Mg-*sg*PPase was incubated with Zn^{2+}, the value of K_m measured with 20 mM Mg^{2+} as the cofactor increased by a factor of 9.7, whereas the values of k_{cat} differed only by a factor of 1.7 (Table 2). One can therefore deduce that Zn^{2+}-induced inactivation of Mg-*sg*PPase (Figure 1) is mainly due to an increase in the K_m to above the concentration of substrate in the assay (50 μM). In contrast, the activation of Mn-*sg*PPase by Zn^{2+} observed when Ca^{2+} was the cofactor (Figure 1) clearly results from increased k_{cat} because K_m was unaffected (Table 2). If Mn-*sg*PPase was assayed in the presence of Mg^{2+}, Zn^{2+} decreased both the k_{cat} and K_m, resulting in virtually no effect on the activity in the presence of 50 μM substrate.

The sedimentation coefficient $s_{w,20}$ measured for Zn-*sg*PPase obtained from Mg-*sg*PPase was 3.9 ± 0.2 S at 26 μM enzyme. This is identical to the value for dimeric Mg-*sg*PPase (*10*). The activity decay seen in Figure 1 is therefore not due to Zn^{2+}-induced dissociation of initially dimeric Mg-*sg*PPase.

Reactivation of Zn-sgPPase by EDTA. Incubation of low-activity Zn-*sg*PPase with EDTA resulted in a slow recovery of activity when measured with Mn^{2+} as the cofactor. Importantly, the reactivation curve shown in Figure 3 exhibited a clear lag phase, characteristic of consecutive reactions. In contrast, the time course of EDTA-induced Zn^{2+} removal from Zn-*sg*PPase did not have a lag phase and perfectly obeyed first-order kinetics with a rate constant of 0.16 ± 0.01 h^{-1} (Figure 3). Thus, Zn^{2+} removal alone is not

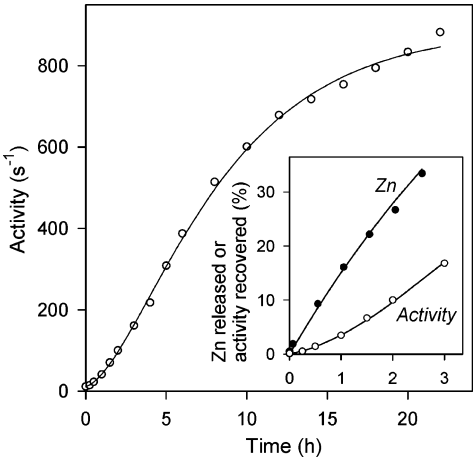

FIGURE 3: Lack of correlation between reactivation of Zn-*sg*PPase and Zn^{2+} removal by EDTA. Two milliliters of Zn-*sg*PPase solution, obtained by a 10-h incubation of 26 μM Mg-*sg*PPase with 30 μM $ZnCl_2$, were mixed with an equal volume of 100 mM EDTA. Aliquots (0.5 mL) were withdrawn at various times and assayed for PPase activity with Mn^{2+} as the cofactor or were subjected to centrifugal ultrafiltration in a Centricon SR10 device for 5 min. The Zn^{2+} content in the eluate was measured by atomic absorption spectroscopy. The lines were obtained with eqs 1−4 using the parameter values listed in Table 3.

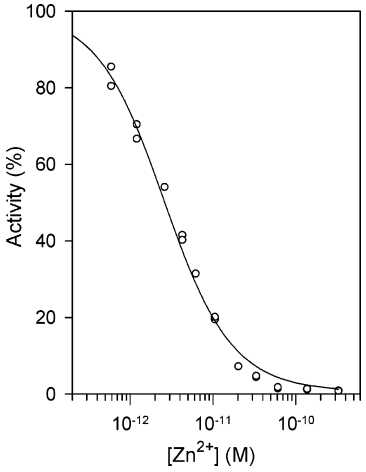

FIGURE 4: Activity of *sg*PPase as a function of the Zn^{2+} concentration in the preincubation medium. Apo-*sg*PPase (26 μM) was incubated for 14 days at 25 °C with $ZnCl_2$ in the presence of 4 mM EGTA in a total volume of 40 μL. Thereafter, aliquots were withdrawn, and PPase activity was assayed with Mn^{2+} as the cofactor. Longer incubations resulted in essentially the same activity values, indicating that equilibrium was attained. The line was obtained with eqs 4−9 using the best-fit parameter values given in text. The value of A_{mn} was taken as 100% activity. The abscissa shows the free metal ion concentration in the preincubation medium as calculated with eqs 5 and 9 using the best fit K_M value of 1.4×10^{-12} M.

Table 3: Parameters of Eqs 1−4 as Estimated from Figures 3 and 5[a]

enzyme	A_{zn} (s^{-1})	$A_{mn/zn}$ (s^{-1})	A_{mn} (s^{-1})	k_r (h^{-1})
*sg*PPase	9 ± 2	100 ± 15	920 ± 20	0.16 ± 0.01
*sm*PPase	12 ± 1	20 ± 15	900 ± 50	0.30 ± 0.03
*bs*PPase	9 ± 1	31 ± 15	110 ± 10	1.8 ± 0.2
HQ97-*bs*PPase	6.0 ± 0.1	5.3 ± 1.1	0.28 ± 0.05	0.52 ± 0.04

[a] All activity assays contained 0.17 mM $MnCl_2$ and 50 μM PP_i.

sufficient to reactivate *sg*PPase, but rather requires additional changes in the enzyme. This behavior is specific to Zn-*sg*PPase because the time course of the activity change when Mn-*sg*PPase was incubated with EDTA did not exhibit a lag phase and obeyed first-order kinetics with a rate constant of 22 h^{-1} (data not shown).

The time courses shown in Figure 3 can be explained by the mechanism described in Scheme 1. This mechanism implies that the two subunits of dimeric PPase lose Zn^{2+} independently with a rate constant k_r of 0.16 h^{-1}, although their activities depend on whether Zn^{2+} is present in the neighboring subunit. The activity assay cofactor (Mn^{2+}) binds to the subsite previously occupied by Zn^{2+}, resulting in three dimeric enzyme species in the activity assay: E_2Zn_2, E_2MnZn, and E_2Mn_2. Fitting eqs 1−4 to the activity curve in Figure 3 revealed that the activity of the Mn^{2+}-bound subunit of the E_2Mn_2-form (A_{mn}) is 9.2-fold higher than that of the Mn^{2+}-bound subunit in the E_2ZnMn-form ($A_{mn/zn}$) (Table 3). Because E_2ZnMn is predominantly accumulated at the initial phase of the reactivation process, this results in a lag in the reactivation curve; in other words, the reaction initially proceeds at a slower rate than a simple first-order reaction.

Binding Affinity of sgPPase for Zn^{2+}. Binding of Zn^{2+} to the high-affinity subsite of *sg*PPase was measured using the method previously described for other divalent metal ions (*10*, *11*). This approach takes advantage of the observation that metal ion binding to the high-affinity subsite (M1) drastically shifts the monomer−dimer equilibrium toward the much more active dimer (Scheme 2) and that the dimer−monomer interconversion is slow compared to the time-scale of the PPase activity assay.

Metal-free enzyme was equilibrated with increasing amounts of $ZnCl_2$, allowing occupation of a fraction of the available high-affinity subsites and, therefore, partial dimerization. The incubation medium included a metal chelator (EGTA), which served as a metal buffer. Enzyme activity was then measured with Mn^{2+} as the cofactor. Mn^{2+} occupies vacant high-affinity subsites and, compared to the time scale of the assay, nearly instantly converts *sg*PPase into the dimeric form (*10*). Consequently, only dimeric E_2Mn_2, E_2ZnMn, and E_2Zn_2 enzyme forms are present in the activity assay medium, like in the EDTA reactivation experiments described above. Fitting eqs 4−9 to the Zn^{2+} titration curve (Figure 4) yielded the following parameter values: $K_M = (1.4 \pm 0.1) \times 10^{-12}$ M, $A_{mn} = 980 \pm 20$ s^{-1}, and $A_{zn} = 9 \pm 1$ s^{-1}. The value of $A_{mn/zn}$ was fixed to 100 s^{-1}, as determined above.

Zn^{2+} Effects on bsPPase and smPPase. As shown in Figure 5, Zn^{2+} had similar effects on the enzyme activities of *sm*PPase and *bs*PPase: (a) the Mg-forms of both enzymes were instantly activated by Zn^{2+}, but the activity subsequently decayed over several minutes in an EDTA-recoverable manner; (b) the EDTA reactivation curves for these enzymes exhibited initial lag phases. Furthermore, Zn^{2+} did not activate the apo-forms of these PPases but slowly activated the Mn^{2+}-form of *bs*PPase (data not shown) as it did with the Mn^{2+}-form of *sg*PPase (Figure 1). The parameter values derived for these enzymes from the inactivation and reactivation curves are summarized in Tables 1 and 3.

Effects of Zn^{2+} on bsPPase Variants. To localize the activating Zn^{2+} ion in the PPase structure, we generated *bs*PPase variants with modified metal-binding subsites M1 (HQ9) and M2 (HQ97, DE15). These were expressed in *E.*

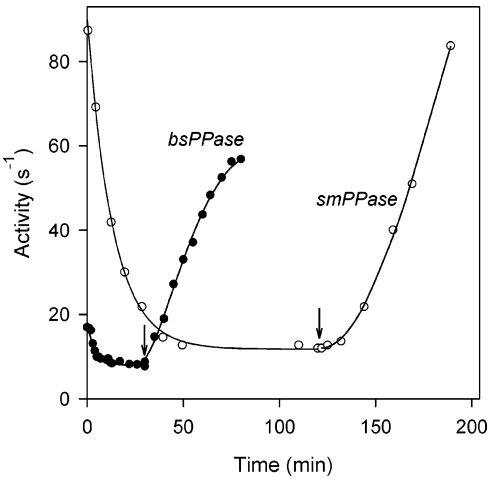

FIGURE 5: Time courses of PPase activity upon addition of 20 μM Mg-*sm*PPase (open circles) or 26 μM Mg-*bs*PPase (closed circles) to a solution of 30 μM $ZnCl_2$. At the time indicated by the arrow, the incubation mixture was diluted 2-fold with 100 mM EDTA solution, and PPase activity was assayed with Mn^{2+} as the cofactor. The final activity of *sm*PPase obtained after 15 h incubation with EDTA was 900 s^{-1}. Mg-PPases were obtained by incubation of 0.1 mM apo-PPases with 0.115 mM $MgCl_2$. The inactivation curves were obtained with eq 10 using the best-fit parameter values given in Table 1, and the reactivation curves were obtained with eqs 1−4 using the best-fit parameter values given in Table 2.

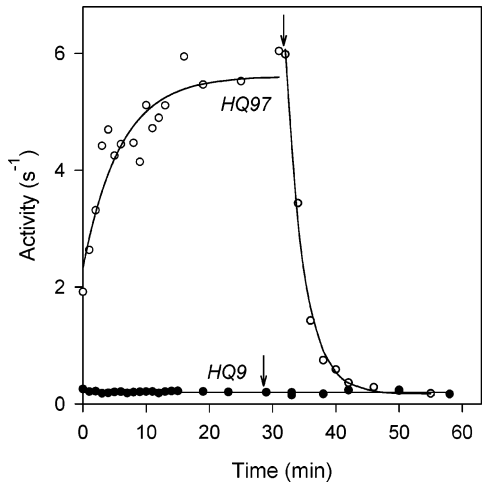

FIGURE 6: Time courses of PPase activity upon addition of 26 μM Mg-form of HQ97-*bs*PPase (open circles) or HQ9-*bs*PPase (closed circles) to a solution of 30 μM $ZnCl_2$. Mg-PPases were obtained by incubation of 0.1 mM apo-PPases with 1.5 mM $MgCl_2$. Otherwise, the experiment was carried out as in Figure 5.

coli, purified, and assayed with various combinations of metal cofactors. Mn^{2+} was used as the cofactor in most of these experiments because it conferred higher activity than Mg^{2+} and Ca^{2+}. Although these variants were 1000-fold less active than wild-type *bs*PPase with Mn^{2+}, we could still reliably measure activity using our assay procedure.

The effects of Zn^{2+} binding and its removal by EDTA were only markedly reduced in the HQ9 Mg-*bs*PPase (Figure 6); however, there was no large qualitative change in the activity curve compared to wild type enzyme (Figure 5). In contrast, the behavior of the HQ97 mutant was significantly different. Specifically, it was slowly activated by Zn^{2+} (Figure 6) like the wild-type Mn-*bs*PPase and Mn-*sg*PPase (Figure 1); rapid transient activation followed by deactivation, characteristic of the wild-type Mg−PPases (Figures 1 and 5), was not observed. EDTA addition inactivated Zn^{2+}-activated HQ97 Mg-*bs*PPase (Figure 6). Furthermore, HQ97 apo-*bs*PPase behaved the same as HQ97 Mg-*bs*PPase, unlike for apo wild-type PPases, which were instantly inactivated by Zn^{2+}. The behavior of the DE15 variant, which is also mutated at the M2 subsite, was similar to that of the HQ97 variant, although the activity increased by only about 40% compared to 140% for the HQ97 variant (Figure 6). Similar effects of Zn^{2+} on these variants were observed when their activities were measured with Mg^{2+} as the cofactor. These results suggest that the M2 subsite is critical for Zn^{2+} modulation of PPase activity and imply that the M2 subsite may be the high-affinity metal-binding site.

Wild-type *bs*PPase is dimeric in the presence of Mg^{2+} or Mn^{2+} as are the HQ9 and DE15 variants, but the HQ97 and HQ98 variants are monomeric (Halonen, P. and Tammenkoski, M., unpublished). To investigate the effect of quaternary structure on Zn^{2+} modulation of *bs*PPase activity, we constructed an R99I variant because this residue is within a β-loop involved in subunit−subunit contact. R99I-*bs*PPase could not dimerize in the presence of Mn^{2+}, as shown by the $s_{20,w}$ value (2.5 ± 0.1 S at 26 μM enzyme, pH 7.2). When measured with Mn^{2+} as the cofactor, the activity of this enzyme was 0.1 s^{-1}, and it either decreased 2-fold (Mg-enzyme) or remained constant (apoenzyme) upon addition of 1.1 equiv of Zn^{2+}. Therefore, it is unlikely that the unusual behavior of the HQ97 variant is due it functioning as a monomer.

DISCUSSION

Family I PPases are Mg^{2+}-dependent enzymes that can use transition metal ions, including Zn^{2+}, as cofactors in vitro. For family II PPases, transition metal ions, together with Mg^{2+}, appear to be in vivo cofactors because they are accumulated by some bacteria that have this type of PPase (*14*, *15*). However, three unique features distinguish the effects of Zn^{2+} from those of other metal cofactors on family II PPases and from the effect of Zn^{2+} on family I PPases: an unusually high binding affinity, low activity of the equilibrium Zn-PPase form, and the transient formation of a highly active Zn-PPase* from Mg-PPase.

Among the metal ions tested (Zn^{2+}, Mn^{2+}, Co^{2+}, Ca^{2+}, and Mg^{2+}), Zn^{2+} binds most tightly to *sg*PPase. The corresponding binding constants, estimated from the effect of metal on enzyme dimerization, are 0.0014, 0.2, 0.67, 5400, and 23 000 nM (*10*, *11*), a range of 10^7. X-ray crystallography shows that this difference arises from the presence of His residues in each of the two metal-binding subsites in the PPase active site (*20*). Specifically, the imidazole group of His is a very good ligand for Zn^{2+}, not as good for Mn^{2+} and Co^{2+}, and unfavorable for Ca^{2+} and Mg^{2+} (*21*). Thus, both the M1 and M2 subsites are expected to tightly bind Zn^{2+}. This prediction is confirmed by the observation that both subsites are occupied in *sg*PPase crystals at low concentrations of Zn^{2+} (*20*). Mn^{2+} binding affinities of the M1 and M2 subsites differ by a factor of 10^6 and are lower than their Zn^{2+}-binding affinities. For Mg^{2+}, the binding affinities of the M1 and M2 subsites are still lower and differ 10^2-fold. The high-affinity subsite appears to be the same for Mn^{2+} and Mg^{2+} (*10*).

The structural data also suggest an explanation for the low activity of Zn-PPase formed from Mg-PPase. In the *sg*PPase•

Mn_2 complex, the metal ion is six-coordinated in the M1 subsite and five-coordinated in the M2 subsite (*20*). On the basis of the structure of *sm*PPase complexed with Mn^{2+} and sulfate, which mimics the binding of P_i, Mn^{2+} appears to also acquire octahedral coordination in the M2 subsite (*7*). Unlike Mg^{2+} and Mn^{2+}, which prefer six-coordination, Zn^{2+} prefers four- or five-coordination. Indeed, in a recently determined structure of the *sg*PPase·Zn_2 complex, Zn^{2+} is four-coordinated in the M1 subsite and five-coordinated in the M2 subsite (*20*). This implies that some of the coordination bonds with sulfate (and, thus, with P_i and PP_i) observed in the dimanganese complex are not formed in the zinc complexes. However, all of these bonds appear to have a role in substrate binding and catalysis. Alternatively, low activity of Zn-PPase may be attributed to a small fraction of active enzyme with six-coordinated Zn^{2+} in equilibrium with the bulk of inactive enzyme having four/six-coordinated Zn^{2+} in the M1 subsite. Interestingly, Cd^{2+}, which also exhibits low coordination numbers (*22*), showed a similar fast transient activation of Mg-*sg*PPase from < 0.1 to 1.3 s^{-1}, followed by a slow inactivation to 0.2 s^{-1} with a rate constant k_c of 0.01 min^{-1}.

To explain Zn^{2+}-induced activity transitions, Mg^{2+} or Mn^{2+} must occupy one metal-binding subsite and Zn^{2+} must occupy the other in the activated enzyme. Differential binding occurs because only one subsite, presumably M2, tightly binds Mg^{2+} and Mn^{2+}, whereas both subsites tightly bind Zn^{2+}. Consequently, preincubation with Mg^{2+} and Mn^{2+} results in an enzyme with the M2 subsite occupied, directing subsequent Zn^{2+} binding to M1. As a result, mixed active enzyme forms arise that have Zn^{2+} at subsite M1 and Mg^{2+} or Mn^{2+} at subsite M2. However, the affinity of the M2 subsite for Zn^{2+} is apparently higher than that of the M1 subsite, resulting in a gradual migration of Zn^{2+} from M1 to M2 and displacement of Mg^{2+}. Accordingly, when equimolar Zn^{2+} is added to apoenzyme, it goes directly to the M2 subsite. Zn^{2+} migration does not occur at the metal concentrations used, or it proceeds much slower when the M2 subsite is occupied by Mn^{2+}, which binds tightly to this subsite. In terms of this mechanism, Zn^{2+} is a poor cofactor at subsite M2 and a good one at subsite M1, and the activating effect of Zn^{2+} on Mg- and Mn-PPase corresponds to formation of a mixed enzyme species containing Zn^{2+} only at subsite M1. The slowness of the Zn^{2+} migration appears to be determined by ligand exchange rate, because the X-ray analysis reported in the accompanying paper in this issue (*20*) revealed no appreciable conformational differences between PPase having Zn^{2+} or Mn^{2+} in its active site.

Ca-PPase was not activated by Zn^{2+}. Instead, like apo-PPase, it was instantly inactivated. This difference in the behavior of Ca-PPase and Mg-PPase might suggest that Ca^{2+} binds to a different subsite (M1), allowing direct binding of Zn^{2+} to M2. In this case, Ca^{2+} would interfere with Zn^{2+} binding to Mn-PPase, but this was not observed. A more likely explanation is that Ca^{2+} is initially located at subsite M2 and that Zn^{2+} readily substitutes for Ca^{2+} due to much faster rates of ligand exchange for Ca^{2+} than for Mg^{2+}. Thus, rates of water exchange differ 500-fold for these cations (3×10^8 s^{-1} versus 6×10^5 s^{-1}, respectively) (*23*).

The effects of Zn^{2+} on *bs*PPase variants, especially HQ97, suggest that M2 is the high-affinity subsite for metal cofactors. Removal of the most important Zn^{2+} ligand in the M2 subsite to give the HQ97 mutation caused a slowing of Zn^{2+}-induced activation of Mg-*bs*PPase, and, more strikingly, allowed Zn^{2+} to activate the apoenzyme even though the wild-type apoenzyme was instantly inactivated by Zn^{2+}. Thus, apo-HQ97-*bs*PPase resembles the wild-type Mn-*bs*PPase, in which the high-affinity subsite is occupied by Mn^{2+}. A simple explanation for this is that M2 is the high-affinity subsite for Mn^{2+} and Mg^{2+}, and, assuming that Zn^{2+} migrates between the two subsites, also for Zn^{2+}. Because His97 of the M2 subsite flanks the interfacial segment (residues 99−115), whereas the M1 subsite is further away, this agrees with the observation that binding of one cofactor ion per subunit markedly stimulates dimerization of family II PPases (*10, 11*). Also, the effect of Zn^{2+} bound to one subunit on the catalytic properties of the other subunit (i.e., the inequality of $A_{mn/zn}$ and A_{mn} in Table 3) supports the idea that Zn^{2+} is located in M2 because it is closer to the subunit interface.

However, this identification of M2 as the high-affinity subsite appears to disagree with recent site-directed mutagenesis studies showing that mutations at the M1 subsite have a greater effect on tight Mn^{2+} binding in the absence of substrate than mutations at the M2 subsite (Halonen P., Tammenkoski, M., unpublished). A possible explanation for this might be that the structurally similar M1 and M2 subsites have roughly similar binding affinities in the metal-free enzyme but that the binding reaction is characterized by a strong negative cooperativity because of electrostatic repulsion of the two bound metal ions (*11*). Indeed, the distance between the metal ions is only 3.6 Å, and they are separated only by a shared water ligand (*7*, *8*). If correct, this binding mechanism would complicate the interpretation of the site-directed mutagenesis data because inactivating one subsite may stimulate binding at the other subsite. Alternatively, distorting the M1 site may affect the structural integrity of the N-terminal domain. The structure of monometal complexes of PPase, currently under study, may help to resolve this question and to unequivocally identify the high-affinity subsite.

ACKNOWLEDGMENT

The authors thank P. V. Kalmykov for assistance with sedimentation velocity measurements.

REFERENCES

1. Kornberg, A. (1962) On the metabolic significance of phosphorolytic and pyrophosphorolytic reactions, in *Horizons in Biochemistry* (Kasha, M., and Pullman, B., Eds.) p 251, Academic Press, New York.
2. Baltscheffsky, M., Schultz, M., and Baltscheffsky, H. (1999) H^+-PPases: a tightly membrane-bound family, *FEBS Lett. 457*, 527−533.
3. Baykov, A. A., Cooperman, B. S., Goldman, A., and Lahti, R. (1999) Cytoplasmic inorganic pyrophosphatase, *Prog. Mol. Subcell. Biol. 23*, 127−150.
4. Heikinheimo, P., Tuominen, V., Ahonen, A.-K., Teplyakov, A., Cooperman, B. S., Baykov, A. A., Lahti, R., and Goldman, A. (2001) Towards a quantum-mechanical description of metal assisted phosphoryl transfer in pyrophosphatase, *Proc. Natl. Acad. Sci. U.S.A. 98*, 3121−3126.
5. Young, T. W., Kuhn, N. J., Wadeson, A., Ward, S., Burges, D., and Cook, J. D. (1988) *Bacillus subtilis* ORF yybQ encodes a manganese-dependent inorganic pyrophosphatase with distinctive

properties: the first of a new class of soluble pyrophosphatase? *Microbiology 144*, 2563−2571.
6. Shintani, T., Uchiumi, T., Yonezava, T., Salminen, A., Baykov, A. A., Lahti, R., and Hachimori, A. (1988) Cloning and expression of a unique inorganic pyrophosphatase from *Bacillus subtilis*: evidence for a new family of enzymes, *FEBS Lett. 439*, 263−266.
7. Merckel, M. C., Fabrichniy, I. P., Salminen, A., Kalkkinen, N., Baykov, A. A., Lahti, R., and Goldman, A. (2001) Crystal structure of *Streptococcus mutans* pyrophosphatase: a new fold for an old mechanism, *Structure 9*, 289−297.
8. Ahn, S., Milner, A. J., Futterer, K., Konopka, M., Ilias, M., Young, T. W., and White, S. A. (2001) The "open" and "closed" structures of the type-C inorganic pyrophosphatases from *Bacillus subtilis* and *Streptococcus mutans*, *J. Mol. Biol. 313*, 797−811.
9. Zyryanov, A. B., Shestakov, A. S., Lahti, R., and Baykov, A. A. (2002) Mechanism by which metal cofactors control substrate specificity in pyrophosphatase, *Biochem. J. 367*, 901−906.
10. Parfenyev, A. N., Salminen, A., Halonen, P., Hachimori, A., Baykov, A. A., and Lahti, R. (2001) Quaternary structure and metal ion requirement of family II pyrophosphatases from *Bacillus subtilis*, *Streptococcus gordonii*, and *Streptococcus mutans*, *J. Biol. Chem. 276*, 24511−24518.
11. Zyryanov, A. B., Vener, A. V., Salminen, A., Goldman, A., Lahti, R., and Baykov, A. A. (2004) Rates of elementary catalytic steps for different metal forms of the family II pyrophosphatase from *Streptococcus gordonii*, *Biochemistry 43*, 1065−1074.
12. Kuhn, N. J., and Ward, S. (1998) Purification, properties, and multiple forms of a manganese-activated inorganic pyrophosphatase from *Bacillus subtilis*, *Arch. Biochem. Biophys. 354*, 47−56.
13. Kuhn, N., Wadeson, A., Ward, S., and Young, T. W. (2000) *Methanococcus jannaschii* ORF mj0608 codes for a class C inorganic pyrophosphatase protected by Co^{2+} or Mn^{2+} ions against fluoride inhibition, *Arch. Biochem. Biophys. 379*, 292−298.
14. Charney, J., Fisher, W. P., and Hegarty, C. P. (1951) Manganese as an essential element for sporulation in the genus *Bacillus*, *J. Bacteriol. 62*, 145−148.
15. Martin, M. E., Byers, B. R., Olson, M. O. J., Salin, M. L., Arceneaux, J. E. L., and Tolbert, C. (1986) A *Streptococcus mutans* superoxide dismutase that is active with either manganese or iron as a cofactor, *J. Biol. Chem. 261*, 9361−9367.
16. Baykov, A. A., and Avaeva, S. M. (1981) A simple and sensitive apparatus for continuous monitoring of orthophosphate in the presence of acid-labile compounds, *Anal. Biochem. 116*, 1−4.
17. Chervenka, C. H. (1972) *Methods for the Analytical Ultracentrifuge*, Spinco Division of Beckman Instruments, Inc., Palo Alto.
18. Dixon, M., Webb, E. C., Thorne, C. J. R., and Tipton, K. F. (1979) *Enzymes*, 3rd ed., pp 144−145, Longman Group Limited, London.
19. Dawson, R. M. C., Elliott, D. C., Elliott, W. H., and Jones, K. M. (1986) *Data for Biochemical Research*, Clarendon Press, Oxford.
20. Fabrichniy, I. P., Lehtiö, Salminen, A., Zyryanov, A. B., Baykov, A. A., Lahti, R., and Goldman, A. (2004) Structural studies of metal ions in family II pyrophosphatases: the requirement for a Janus ion, *Biochemistry 43*, 14403−14411.
21. Bock, C. W., Katz, A. K., Markham, G. D., and Glusker, J. P. (1999) Manganese as a replacement for magnesium and zinc: functional comparison of the divalent ions, *J. Am. Chem. Soc. 121*, 7360−7372.
22. Venkataraman, D., Du, Y., Wilson, S. R., Hirsch, K. A., Zhang, P., and Moore, J. S. (1997) A coordination geometry table of the *d*-block elements and their ions. *J. Chem. Educ. 74*, 915−918.
23. Smith, D. (1995) Magnesium as the catalytic center of RNA enzymes. in *The Biological Chemistry of Magnesium* (Cowan, J. A., Ed.) pp 111−137, VCH Publishers, Inc., New York.

BI048470J